A numerical model for sound propagation through a turbulent atmosphere near the ground

P. Chevret,[a] Ph. Blanc-Benon, and D. Juvé
Laboratoire de Mécanique des Fluides et d'Acoustique de l'Ecole Centrale de Lyon, U.M.R. C.N.R.S. 5509-B.P.163, 69131 Ecully Cedex, France

(Received 5 September 1995; revised 7 July 1996; accepted 10 July 1996)

In this paper a series of numerical simulations of the effect of turbulence on the propagation of acoustic waves in the atmosphere are presented. First the technique of representing the turbulence as a set of realizations of a random field generated by a limited number of Fourier modes is described. Through each individual realization, the acoustic waves are propagated in a wide-angle parabolic approximation to obtain the sound-pressure level. Ensemble averaging is then performed to compute the statistical properties of the acoustic field: mean sound-pressure level, intensity fluctuations, and amplitude distributions. The method is applied first to a nonrefractive atmosphere, both in the presence of a rigid boundary and of an impedance ground, and then to an upward refractive atmosphere with an impedance ground. The model, which contains no adjustable parameters, is tested using the experimental data of Parkin and Scholes, Daigle, and Wiener and Keast. Good agreement between numerical simulations and experiments is obtained.

PACS numbers: 43.28.Fp, 43.20.Bi, 43.20.Fn, 43.50.Vt [LCS]

INTRODUCTION

Atmospheric turbulence causes random fluctuations in temperature, wind velocity, pressure, and density. When an acoustic wave is propagated through a turbulent atmosphere, its amplitude and phase are significantly affected by the variations in the value of the refraction index along the propagation path. The influence of temperature and wind velocity variations has been demonstrated in many experimental studies.[1,2] From these measurements, it is clear that the effect of turbulence is particularly important in two situations:

(1) Propagation near the ground at small distances where the partial loss of coherence between the direct and the reflected paths induces a reduction of the interferences. The acoustic levels measured at a minimum can be increased by 10 dB.[3–5]

(2) Propagation over long distances when strong negative vertical sound speed gradients refract sound upward. Deterministic computations predict the existence of a deep shadow zone, whereas measurements indicate a nonnegligible sound-pressure level due to the scattering of sound by turbulence.[6]

Theoretical analyses of waves, including acoustic waves, propagating in random media have been extensively treated, but analytical results are usually limited to the case of an unbounded medium with an homogeneous deterministic background.[7] For a nonrefracting atmosphere, Daigle presented a model to predict the field of acoustic waves produced by a point source propagating in a turbulent atmosphere above a hard[5] or a finite impedance boundary.[8] Daigle's analysis is an extension of the weak scattering theory developed by Chernov[9] for homogeneous and isotropic turbulence. An important parameter of this approach is the correlation coefficient between the direct and reflected waves which has to be adjusted according to experimental data. This theory is limited to short-range propagation and weak fluctuations of the refraction index.

In recent years several authors have taken into account the effect of turbulence on sound propagation through numerical simulations.[10–12] The basic idea is to model the turbulence as a set of independent realizations of a random field; for each realization, deterministic equations are solved to obtain the acoustic pressure field. Then, the relevant statistical quantities (mean sound-pressure levels, amplitude fluctuations, etc.) are computed by averaging over an ensemble of realizations. In the model of McBride *et al.*[12] the atmospheric turbulence is described as an ensemble of random spherically symmetric eddies with Gaussian index of refraction profiles. For each realization, the total sound pressure is calculated by coherently adding the individual scattering contributions of each eddy or ''turbule.'' The scattered field of each turbule is obtained using a Born approximation or a Rytov method for higher frequencies. Even though this approach is in good agreement with experimental studies reported in the literature, its domain of validity is limited by the use of scattering theories which break down for long-range propagation. A different approach to take into account the atmospheric turbulence is to split the refraction index n into two components, i.e., a mean part $\langle n \rangle = c_0/c$ (c_0 is the reference sound speed and c is the mean local sound speed) and a random part μ related to the fluctuations of the medium. Then, assuming that the time evolution of the turbulent structures is much greater than the transit time of the acoustic wave, it is possible to represent the index fluctuations μ as a set of independent realizations of a spatially random field. In the model developed by Gilbert *et al.*,[10] the realizations of μ

[a]Presently at: CPE Lyon, LISA (CNRS EP0092)/LASSSO, Laboratoire d'Acoustique, Systèmes, Signaux et SOnar, 25 rue du Plat, 69288 Lyon Cedex 02, France.

are calculated as the output of a filter excited by white noise. The properties of the filter are chosen according to the turbulent parameters, such as the correlation length, the correlation function of the index fluctuations, and the level of these fluctuations. Then, the acoustic wave is propagated using a parabolic equation method. This approach gives useful predictions for the calculation of turbulent effects in an upward-refracting atmosphere with long-range propagation and frequencies above a few hundred Hz.[10] An alternative model of ''cheap'' turbulence has been introduced by Blanc-Benon *et al.*[13] The hypothetical turbulent field consists of a small number of randomly oriented, discrete, Fourier modes whose amplitudes are chosen to produce a distribution of temperature or velocity comparable to those found in the experimental studies. It has been applied successfully to the random focusing of waves in turbulence,[14] the propagation of waves through homogeneous unbounded turbulent media,[15] and the sound propagation in the atmosphere.[16] In this paper we present a systematic application of the random Fourier modes technique to sound propagation in the near ground atmosphere. In Sec. I we outline the basic ideas of the synthetized turbulence model and the wide-angle parabolic equation method. In Sec. II, we present numerical simulations for a nonrefracting atmosphere. Predictions for the relative sound-pressure levels are compared with experimental data reported by Parkin and Scholes[3,4] and Daigle *et al.*[5] In Sec. III, we consider the upward-refracting atmosphere case with reference to the experiments of Wiener and Keast.[6] The physical phenomena involved are qualitatively illustrated by snapshots of the scattered acoustic field in the shadow zone. Quantitative comparisons are made between the parabolic computations and data for the relative sound-pressure level versus range. Finally, some results are presented for the intensity fluctuations and for the probability density function of the pressure amplitude. Section IV gives a summary and conclusions.

I. THEORETICAL BACKGROUND

Our numerical simulation of sound waves through turbulence involves two elements; the generation of a random field in terms of a superposition of discrete random Fourier modes and the integration of a deterministic wave equation. The sound field can then be characterized by ''instantaneous'' maps of the sound-pressure level and by statistical properties obtained using an ensemble average.

A. Modeling the turbulent field

Here we consider that the temperature fluctuations in the atmosphere are the only cause of the fluctuations of the sound speed c. Assuming that the turbulence is frozen in time, the temperature fluctuations T' at a point $\mathbf{x}$ can be represented by a sum of N random Fourier modes,

$$T'(\mathbf{x}) = \sum_{j=1}^{N} \mathscr{T}(\mathbf{K_j}) \cos(\mathbf{K_j}\cdot\mathbf{x} + \varphi_j). \tag{1}$$

Here, $\mathscr{T}(\mathbf{K_j})$ and φ_j are the amplitude and the phase angle of the jth Fourier mode and $\mathbf{K_j}$ is the turbulent wave vector. For a two-dimensional field, each vector $\mathbf{K_j}$ is defined in Fourier space by its modulus K_j and its orientation θ_j (see Fig. 1). One of the advantages of this technique is its ability to generate random fields of infinite extent with prescribed spectra. In addition, since the turbulent fields have been modeled in terms of a fixed number of discrete Fourier modes, we can derive analytically the fields and their spatial derivatives at every point $\mathbf{x}$. The index of refraction n is then expressed in terms of a mean part $\langle n\rangle = c_0/c$ and a fluctuating part $\mu = -T'/2T_0$ (T_0 is the reference temperature). We simplify the problem by assuming that $\langle n\rangle$ varies only with the height z above the ground and that $T'(\mathbf{x})$ is a function of z and the horizontal distance r. Although the present work deals with two-dimensional scalar random fields, its extension to three-dimensional scalar or vectorial fields presents no special difficulties.[15,17]

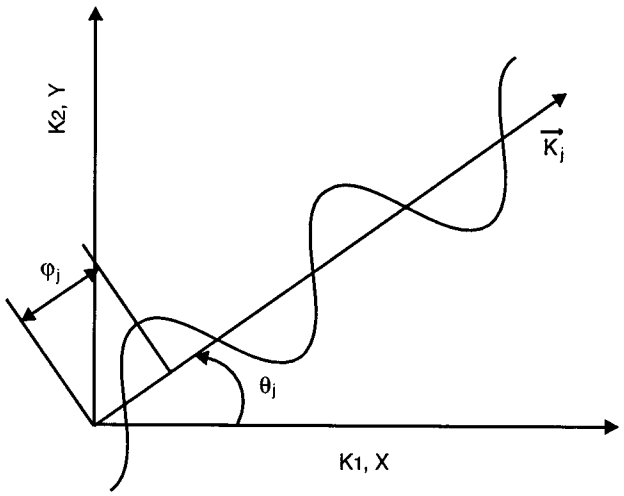

FIG. 1. Sketch of one Fourier mode.

In this paper the turbulence is considered isotropic and homogeneous and the spectral density of the turbulent eddies is modeled with a Gaussian distribution. Even though it is a simple model for atmospheric turbulence near the ground, this approximation has been used successfully by Daigle *et al.*[18,19] to explain outdoor sound propagation experiments. It has also been introduced in numerical simulations to predict the effects of turbulence in an upward-refracting atmosphere by Gilbert *et al.*[10] and Havelock *et al.*[20] In a future paper we will report on the influence of turbulence model in predicting sound-pressure levels in a refractive shadow zone.

To obtain a statistically homogeneous and isotropic field T', angles θ_j and φ_j must be independent random variables with uniform distribution over $[0,2\pi]$. The amplitude of each mode is picked from a prescribed energy spectrum $G(K)$. $G(K)$ is related to the two-point temperature correlation $m(r)$ by[14]

$$G(K) = \theta^2 K \int_0^{+\infty} r m(r) J_0(Kr)\, dr, \tag{2}$$

where θ^2 is the variance of the temperature fluctuations and J_0 is the Bessel function of first kind and zero order. In our numerical simulations, $G(K)$ is sampled uniformly by N val-

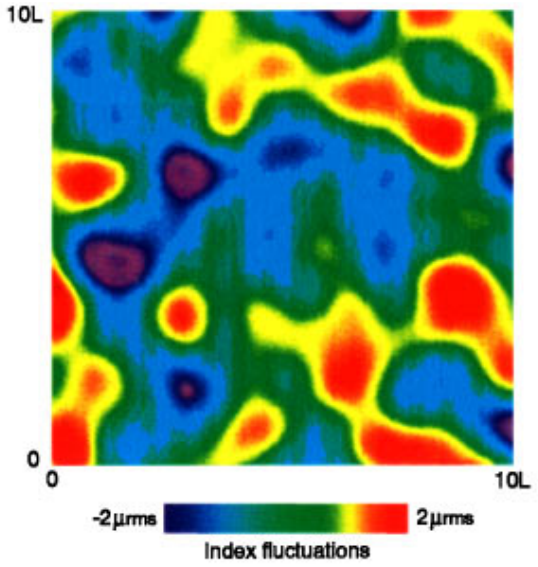

FIG. 2. One realization of the refraction index field ($K_{\min}=0.1/L$ m^{-1}, $K_{\max}=6/L$ m^{-1} and 100 modes). The index fluctuations μ are plotted using a color scale which extends from -2 to 2 times the rms. value of μ.

ues K_j between a minimum value $K_{\min}$ and a maximum value $K_{\max}$, chosen so that the energy of the turbulent structures is well represented. In this study, the random field $T'(\mathbf{x})$ is characterized by a Gaussian correlation function $m(r)$:

$$m(r)=\exp(-r^2/L^2), \tag{3}$$

where L is related to the integral scale of the turbulence $l_{\text{int}}(l_{\text{int}}=\sqrt{\pi}/2L)$. The associated energy spectrum is given by

$$G(K)=\frac{\theta^2}{4}KL^2\exp\left(-\frac{K^2L^2}{4}\right). \tag{4}$$

In Fig. 2, we present a map of the index fluctuations μ obtained for a typical realization of a ''Gaussian turbulence.'' The number of modes N is 100; the minimum value $K_{\min}$ and the maximum value $K_{\max}$ are respectively $0.1/L$ and $6/L$ with $L=1$ m. The rms. value of the refraction index fluctuations is equal to 10^{-3}. The spatial extent of the visualized field is $10L\times10L$. This map shows ''hot'' (red spot) and ''cold'' (blue spot) structures whose size is of the same order of magnitude as the characteristic length L. We note that the boundary of each of these inhomogeneities is very smooth, as is the transition between hot and cold structures.

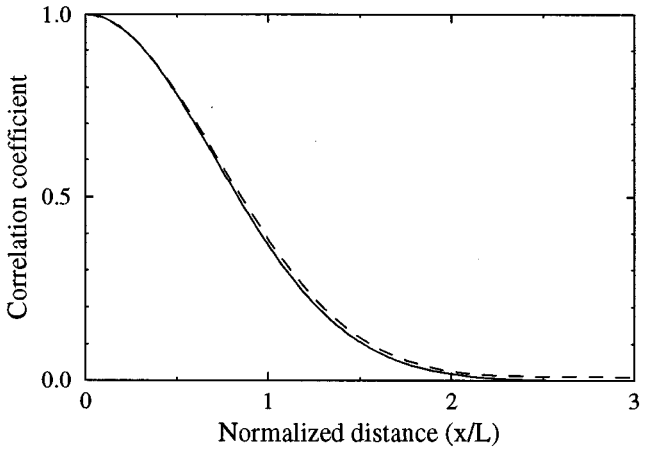

FIG. 3. Correlation coefficient: comparison between the exact (———) form and our model (-----).

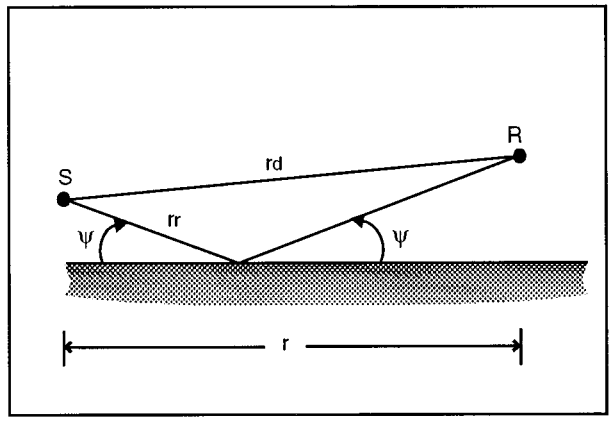

FIG. 4. Superposition of the direct and the ground reflected waves.

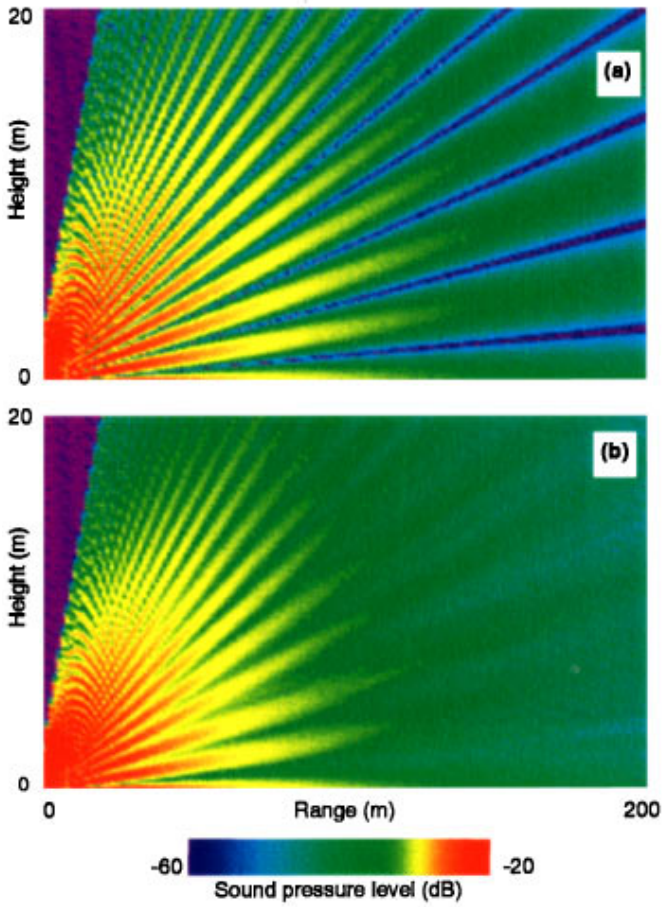

FIG. 5. Sound-pressure level near a rigid boundary, for a nonturbulent (a) and a turbulent (b) atmosphere ($f=4000$ Hz, $h_s=1.2$ m, $\langle\mu^2\rangle=7.7\times10^{-6}$, $L=1.1$ m, 50 realizations).

After averaging over an ensemble of such realizations, the second-order statistical properties of the turbulence can be recovered. Figure 3 presents a comparison between the exact Gaussian correlation [Eq. (3)] and the estimated one. The agreement is excellent. Additional details for homogeneity, isotropy, and correlation length of the turbulent field are given by Hugon-Jeannin.[15]

B. The computation of the sound field

For the prediction of the sound field, we have developed a code based on the parabolic equation method. The parabolic equation, first introduced in underwater acoustics, was originally limited to narrow-angle propagation; in the last decade it has been improved to handle wide-angle propagation problems and is now established as an efficient approximation of the Helmholtz equation.[21,22] For atmospheric environments with a realistic range-dependent description of the atmosphere, including turbulence and ground effects, the parabolic equation method has been used first by Gilbert *et al.*[10] and then by Juvé *et al.*[16] In this section we briefly summarize the derivation of the wide-angle equation used in our model. The details of the method can be found in Chevret.[23]

The starting point is the Helmholtz equation for a harmonic point source of strength $\mathcal{S}$ in an environment with azimuthal symmetry:

$$\left(\frac{\partial^2}{\partial r^2}+\frac{1}{r}\frac{\partial}{\partial r}+\frac{\partial^2}{\partial z^2}+k_0^2 n^2\right)P(r,z)=\mathcal{S}\delta(\mathbf{x}-\mathbf{x}_0), \tag{5}$$

where $P(r,z)$ is the acoustic pressure, k_0 is the reference wave number, $\mathbf{x}_0=(r_0,z_0)$ is the position of the source, δ is the Dirac function, and n is the index of refraction composed of a deterministic part $\langle n\rangle$ and a random part μ. The farfield approximation of Eq. (5) is

$$\left(\frac{\partial^2}{\partial r^2}+\frac{\partial^2}{\partial z^2}+k_0^2 n^2\right)u(r,z)=0, \tag{6}$$

where u is the variable $\sqrt{r}P(r>0)$.[10] For weak turbulence ($\mu_{\rm rms}\ll 1$), the backscattering by index fluctuations is very small and the acoustic field is dominated by forward propagating waves. The outgoing waves are solutions of the following one-way wave equation:

$$\frac{\partial}{\partial r}\Psi(r,z)=ik_0(Q-1)\Psi(r,z), \tag{7}$$

where $\Psi(r,z)$ is the envelope $\Psi(r,z)=u(r,z)\exp(-ik_0 r)$ and Q is the square root of the linear second-order operator Q^2 defined as

$$\begin{aligned} Q^2&=n^2+\frac{1}{k_0^2}\frac{\partial^2}{\partial z^2}=1+\mathscr{L},\\ \mathscr{L}&=(n^2-1)+\frac{1}{k_0^2}\frac{\partial^2}{\partial z^2}. \end{aligned} \tag{8}$$

The main difficulty in solving Eq. (7) is writing an accurate analytical development of the operator Q. For atmospheric sound propagation, numerical solutions can be obtained using finite-difference discretization,[24] a split-step Fourier algorithm, or a Green's function method.[25] For sound propagation in a turbulent atmosphere, the computational efficiency of the Green's function method can be maintained using a phase screen method to describe the random component of the index of refraction.[26] In this paper we decided not to use this phase screen approach to be sure that the small-scale structures of the turbulence, which may have significant contributions to the scattering of waves for large angular deviations from the main axis of propagation, will be numerically tracked by the algorithm.

The principle of the method we used was first presented by Saad and Lee[27] for underwater acoustic propagation. The extension to wide-angle approximation using a higher-order Padé development was done by Collins.[22] Next we outline the necessary steps of this method. To advance the solution of Ψ over a short-range Δr, we assume that the operator $Q=\sqrt{1+\mathscr{L}}$ is slowly varying with range. Then, locally, the formal solution to Eq. (7) takes the form

$$\psi(r+\Delta r,z)=\exp[ik_0(Q-1)\Delta r]\psi(r,z). \tag{9}$$

The exponential operator is approximated by a rational approximation. Following Saad and Lee,[27] we use a second-order Padé development which yields

$$\exp[ik_0\Delta r(\sqrt{1+\mathscr{L}}-1)]\sim\frac{1+p_1\mathscr{L}+p_2\mathscr{L}^2}{1+q_1\mathscr{L}+q_2\mathscr{L}^2}, \tag{10}$$

where the coefficients p_1, p_2, q_1, and q_2 are expressed in terms of the parameter $\sigma=ik_0\Delta r$ as

$$\begin{aligned} p_1&=\frac{3+\sigma}{4}, \quad p_2=\frac{\sigma^2+6\sigma+3}{48},\\ q_1&=\frac{3-\sigma}{4}, \quad q_2=\frac{\sigma^2-6\sigma+3}{48}. \end{aligned}$$

According to the analysis of Saad and Lee,[27] the stability of the derived numerical scheme is guaranteed by imposing that the numerator and the denominator of the rational approximation are complex conjugates of each other, so that the resulting rational function [Eq. (10)] is always of modulus one. Replacing the approximation (10) for the exponential term in Eq. (9), we obtain the formal expression for the one-way equation:

$$\begin{aligned} &[1+q_1\mathscr{L}+q_2\mathscr{L}^2]\psi(r+\Delta r,z)\\ &\quad=[1+p_1\mathscr{L}+p_2\mathscr{L}^2]\psi(r,z). \end{aligned} \tag{11}$$

Numerically, this leads to an implicit integration scheme of the form

$$[1+q_1\mathscr{L}_h+q_2\mathscr{L}_h^2]\psi_h^{n+1}=[1+p_1\mathscr{L}_h+p_2\mathscr{L}_h^2]\psi_h^n. \tag{12}$$

Here $\mathscr{L}_h$ and $\mathscr{L}_h^2$ represent the centered difference approximations to the partial differential operators $\mathscr{L}$ and $\mathscr{L}^2$ with respect to the variable z. This corresponds to a linear system with pentadiagonal matrices. The resolution is performed with a standard LU decomposition method.[28] This second-order Padé scheme can accommodate a propagation angle as high as 54°, which is a wider angle than existing finite-difference techniques having similar cost per step (see the extensive analysis of Saad and Lee[27]). We used a vertical

step Δz of $\lambda/4$ and a horizontal marching step Δr of λ.[23] The ground is modeled as a flat locally reacting plane with a complex impedance; a nonreflecting boundary condition is imposed at the top of the computational domain by adding an absorption layer of several wavelengths thickness, so that no significant energy is artificially introduced by reflection from the upper boundary of the mesh. For the initial pressure field we use a Gaussian starter with adjustable width to simulate the radiation of a point source. The stability and precision of our numerical scheme has been tested for sound propagation along an impedance boundary in an homogeneous medium. An excellent agreement with the analytical asymptotic solution of Attenborough *et al.*[29] has been obtained.

II. COMPARISONS WITH OUTDOOR MEASUREMENTS IN THE LINE OF SIGHT REGION

When the sound source and the receiver are placed above a flat ground, in a nonrefractive atmosphere the acoustic wave reaches the receiver via two paths: (1) directly from the source to the receiver and (2) after being reflected from the ground surface (Fig. 4). The superposition of the direct and the reflected waves induces pronounced interferences which are a function of the frequency; the height of the source and of the receiver, their horizontal separation, and the nature of the ground are additional important parameters. In the case of a wave propagating over a hard boundary, interferences are only a function of the frequency and of the path difference between the direct and the reflected rays. Very low sound-pressure levels are obtained at the receiver when the phase difference between the two trajectories is equal to $(2m+1)\pi$ (m being an integer). When the ground surface impedance is finite and complex, phase and magnitude changes are observed for the reflected sound field. The total pressure field also exhibits typical interference patterns. This qualitative discussion is in agreement with all the experiments conducted in a steady atmosphere. However, if the atmosphere becomes random, the sound-pressure levels measured at the exact location of the interference minima are significantly higher than the values predicted by a deterministic computation.[1] In this section we compare the predictions of our model for sound-pressure levels in a turbulent atmosphere with outdoor measurements. This comparison is completed with analytical and numerical (scatter plots) results concerning the fluctuations of the acoustic pressure field. The study is split into two parts: the propagation over a rigid boundary and the propagation over a finite impedance ground.

A. Sound propagation over a rigid boundary

In this case extensive measurements have been made by Daigle *et al.*[5] Here we focus particularly on two series of their data. For both experiments the source is located at 1.2 m above the ground and the distance between the source and the receiver is 15 m. In the first series the receiver is placed at 0.6 m over the ground, and in the second one it is located at the height of the source, i.e., 1.2 m. According to meteorological measurements reported by Daigle *et al.*,[5] the variance of the refraction index $\langle\mu^2\rangle$ is equal to 7.7×10^{-6} and the characteristic length L of the turbulent structures is equal to 1.1 m. The sound-pressure levels have been measured for a source frequency range between 1 kHz and 6 kHz.

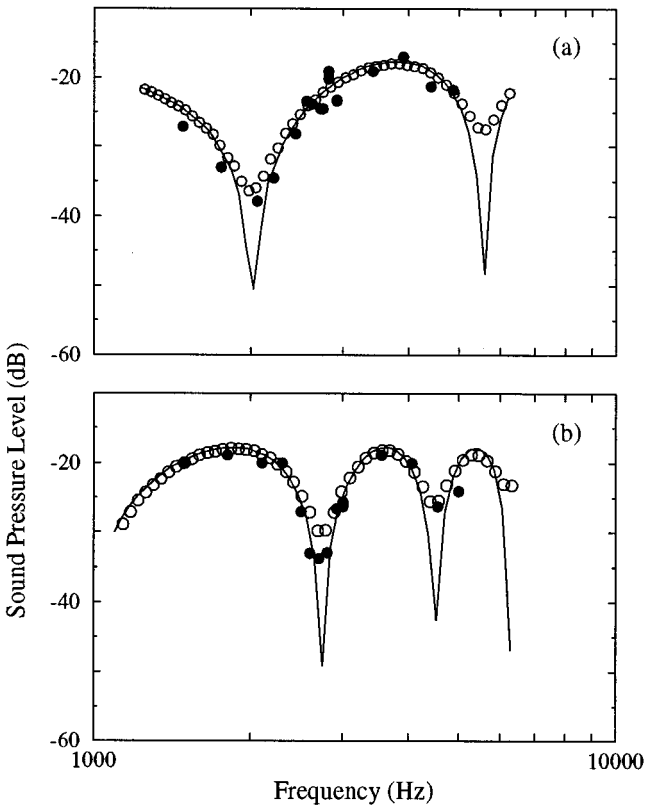

FIG. 6. Sound-pressure level spectrum: comparison between Daigle's measurements (●), a deterministic calculation (———) and our model (○) [$\langle\mu^2\rangle=7.7\times10^{-6}$, $L=1.1$ m, $r=15$ m, $h_s=1.2$ m, (a) $h_r=0.6$ m, (b) $h_r=1.2$ m].

In the absence of a mean sound-speed gradient, the main effect of the turbulence is to blur the pattern produced by the interferences between the direct and the reflected waves. This effect is illustrated in Fig. 5. The frequency is 4 kHz, the distance of propagation is 200 m, and the height of the domain is 20 m. For a nonturbulent atmosphere, the interference pattern is clearly marked with a reduction of sound-pressure levels of 60 dB or more in the region of destructive interferences. For a turbulent atmosphere, the mean pressure level is computed by averaging over 50 realizations. We note that as the distance of propagation increases, the characteristic interference pattern disappears; for a distance greater than 100 m the acoustic field is practically homogeneous, as we demonstrate analytically later [e.g., Eqs. (17) and (18)].

For quantitative comparisons with the measurements reported by Daigle *et al.*,[5] we considered the sound-pressure level at a fixed receiver position with a varying source frequency for two heights of the receiver h_r (0.6 m, 1.2 m). In Fig. 6 we have superposed the results for the deterministic case and the turbulent one; the averaging has been made over a relatively small number of realizations, i.e., 50. A fast convergence of the results has been observed for all the practical cases studied.[15,23] We explain this behavior by the fact that the acoustic wave propagates over a large number of charac-

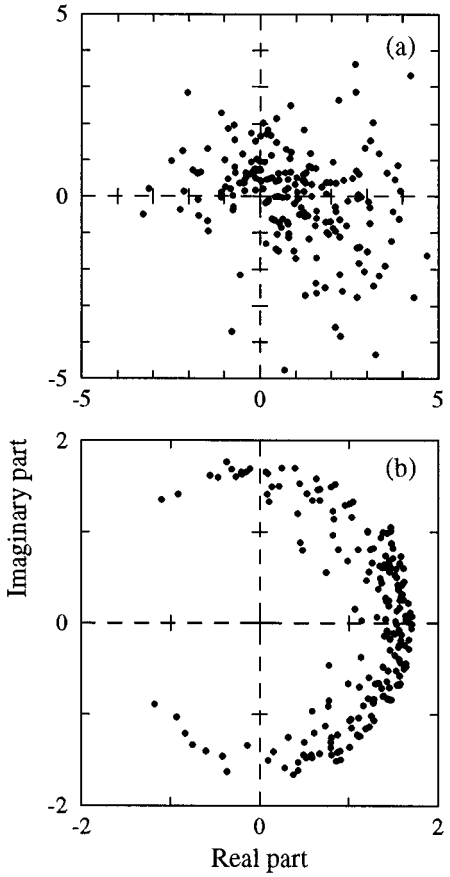

FIG. 7. Scatter plots of the normalized acoustic pressure field (a) in a destructive interference, $f=4500$ Hz; (b) in a constructive interference, $f=3500$ Hz. ($\langle\mu^2\rangle=7.7\times10^{-6}$, $L=1.1$ m, $r=15$ m, $h_s=h_r=1.2$ m.)

teristic scales L, leading to an additional spatial averaging connected to the cumulative effect of turbulence. The two plots of Fig. 6 show very good agreement between the data of Daigle *et al.*[5] and our model for a wide frequency range. We note especially the filling-in of the interference minima where an increase in sound-pressure level up to 20 dB is observed. However, at the first interference minimum in case (b), our simulation overpredicts the measured level by more than 5 dB. The reasons for this discrepancy are not clear but may involve 3-D effects and small deviations of the experiment spectrum from the Gaussian shape. We point out the fact that all the meteorological parameters used in our simulations have been taken from outdoor measurements without any empirical adjustment. However, we have determined that small deviations ($\pm10\%$) from the given values of L or $\langle\mu^2\rangle$ have no perceptible effects on the sound-pressure level spectra.[23] In curve (b), we note also a small reduction of the predicted level in the regions of constructive interferences. This reduction increases with frequency as scattering of the acoustic wave increases; a reduction of 2 dB is obtained for the highest frequencies.

To complete the interpretation of these results it is interesting to consider the fluctuations of the pressure at a given point. In Fig. 7 we have plotted two ''scatter'' plots of the normalized pressure $p/\langle p\rangle$, where $\langle p\rangle$ is the mean field or coherent part of the wave. In these plots the coordinates are the real and the imaginary parts of $p/\langle p\rangle$, as introduced by McBride *et al.*[12] The receiver is located at the same height as the source, 1.2 m, and at a distance r of 15 m. Depending on the frequency of the source, we obtained a destructive interference [$f=4.5$ kHz, Fig. 7(a)] or constructive interference [$f=3.5$ kHz, Fig. 7(b)]. In these diagrams each point is associated with one realization of the random medium. The first scatter plot shows a large spreading of data, whereas the second gives a set of points localized around a circular arc of radius 1.6. We also note that the points are mainly located in the half-plane $\mathrm{Re}(p/\langle p\rangle)\geqslant 0$. These results can be understood by a simple analytical analysis of the pressure field. For these experimental data the wave parameter $D=r/k_0L^2$ is equal to 0.15 for $f=4.5$ kHz and to 0.19 for $f=3.5$ kHz. Thus, D is smaller than 1 and it is possible to evaluate the mean field $\langle p\rangle$ using a geometric approximation method (see the Appendix for details). When the position of the receiver corresponds to a constructive interference, the modulus of $p/\langle p\rangle$ is given by Eq. (A9):

$$\left|\frac{p}{\langle p\rangle}\right|\simeq\exp\left(\frac{\sqrt{\pi}}{2}\langle\mu^2\rangle k_0^2Lr\right). \tag{13}$$

In the plane ($\mathrm{Re}(p/\langle p\rangle)$, $\mathrm{Im}(p/\langle p\rangle)$) this corresponds to a circle with a radius equal to 1.55 in the case of the data reported by Daigle *et al.*[5] This result is in very good agreement with our numerical simulation [see Fig. 7(b)]. The sign of the real part of $p/\langle p\rangle$ [Eq. (A13)] is given by the sign of the product $\cos[(S_r+S_d)/2]\times\cos[(S_r-S_d)/2]$. For short distances ($r=15$ m), the phase fluctuations S_r and S_d are small and have the same order of magnitude; consequently the expression $\cos[(S_r+S_d)[2]]\times\cos[(S_r-S_d)/2]$ will be positive for almost all of the realizations, as clearly shown on Fig. 7(b).

When the position of the receiver corresponds to a destructive interference, the differences (S_r-S_d) and $(\sigma_{S_r}^2-\sigma_{S_d}^2)$ are small for the experimental configuration and the modulus of $p/\langle p\rangle$ can be approximated by [Eq. (A11)]:

$$\left|\frac{p}{\langle p\rangle}\right|\simeq 2\exp\left(\frac{\sigma_{S_d}^2}{2}\right)\frac{|S_r-S_d|}{|\sigma_{S_d}^2-\sigma_{S_r}^2|}. \tag{14}$$

As $|\sigma_{S_d}^2-\sigma_{S_r}^2|$ is very small a large variation of the modulus $|p/\langle p\rangle|$ can be obtained depending on the instantaneous phase difference S_r-S_d. This gives a wide spatial distribution on the scatter plot diagram [see Fig. 7(a)]. The sign of the real part of $p/\langle p\rangle$ [Eq. (A14)] is governed by the sign of the product $\sin[(S_r+S_d)/2]\times\sin[(S_r-S_d)/2]$. This sign is strongly dependent of the instantaneous phase difference, as confirmed by the scatter plot [Fig. 7(a)].

Let us now consider the evolution of the mean-square pressure with the distance of propagation. In their analytical analysis, Daigle *et al.*[5] have shown that $\langle p^2\rangle$ can be written as

$$\langle p^2\rangle = \frac{2}{r_d r_r}\left[\frac{\sigma_A^2}{2}\left(\frac{r_r}{r_d}+\frac{r_d}{r_r}\right)+\frac{r_r}{2r_d}\left(1-\frac{r_d}{r_r}\right)^2 + 1+(1-\sigma_A^2\rho_A)\cos[k_0(r_r-r_d)]\exp[-\sigma_S^2(1-\rho_S)]\right]. \tag{15}$$

σ_A^2 and σ_S^2 are, respectively, the amplitude and the phase variance of each wave ($\sigma_A^2 \simeq \sigma_{A_r}^2 \simeq \sigma_{A_d}^2$; $\sigma_S^2 \simeq \sigma_{S_r}^2 \simeq \sigma_{S_d}^2$). ρ_A and ρ_S are the amplitude and phase correlation coefficients between the direct and the reflected paths. As previously, we assume that $r_r/r_d \simeq 1$ and $\sigma_A^2 \ll 1$ and we write $\langle p^2\rangle$ in the form

$$\langle p^2\rangle = \frac{2}{r^2}\{1+\cos[k_0(r_r-r_d)]\exp[-\sigma_S^2(1-\rho_S)]\}. \tag{16}$$

Depending on the location of the receiver, $\langle p^2\rangle$ will oscillate between the following values:

$$\langle p^2\rangle_{\max} = \frac{2}{r^2}\{1+\exp[-\sigma_S^2(1-\rho_S)]\}, \tag{17}$$

$$\langle p^2\rangle_{\min} = \frac{2}{r^2}\{1-\exp[-\sigma_S^2(1-\rho_S)]\}. \tag{18}$$

The phase variance σ_S^2 [Eq. (A8)] increases with the frequency of the source, and the distance from the source. As a consequence, as frequency and/or range increases, the maximum intensity level will decrease for a constructive interference [Eq. (17)] and increase for a destructive interference [Eq. (18)]. This is in agreement with the results of Fig. 6. For increasing distances, the variance σ_S^2 becomes large and the limit value of both expressions (17) and (18) is $2/r^2$. This value corresponds to the incoherent sum of the direct and the reflected waves. The field becomes homogeneous for large distances of propagation and high frequencies, as clearly shown in Fig. 5.

B. Sound propagation over a finite impedance boundary

In our computations the ground is modeled as a flat plane with finite complex impedance Z_s. Z_s is calculated using the one parameter formula of Delany-Bazley:[30]

$$Z_s = \rho_0 c_0\left[1+0.05\left(\frac{\rho_0 f}{\sigma}\right)^{-0.75}+i0.077\left(\frac{\rho_0 f}{\sigma}\right)^{-0.73}\right], \tag{19}$$

where ρ_0 is the air density, c_0 is the sound speed, and σ is the flow resistivity [formula (19) is expressed in mks units]. For our comparisons, we referred to the experimental studies of Parkin and Scholes[3,4] which were made under homogeneous atmospheric conditions (i.e., no wind and temperature gradients). The source and the receiver are, respectively, located at 1.8 m and 1.5 m above the ground. The frequency is in the range 100 Hz–3 kHz. The ground is covered with grass (flow resistivity $\sigma = 3\times10^5$ Nm^{-4} s). The turbulence is characterized by a variance $\langle\mu^2\rangle$ of 2×10^{-6} and a scale of inhomogeneities L of 1.1 m. These are the estimated values obtained by Daigle[8] in his analysis of the experimental data of Parkin and Scholes. In Fig. 8 our numerical simulations are compared with a deterministic calculation and experimental data for two propagation distances: $r = 200$ m and $r = 350$ m. For both curves, a pronounced minimum occurs between 400 Hz and 600 Hz. This excess attenuation band becomes larger and stronger when the distance r increases: 20 dB at 200 m [Fig. 8(a)] and 25 dB at 350 m [Fig. 8(b)]. The interference of the direct and ground reflected waves, which depends on the exact phase relationship between them, is strongly affected by turbulence. For high frequencies (above 400 Hz), the deterministic calculations overpredict the attenuation of the sound pressure. The discrepancy between the measured points and the solid curve increases with the distance of propagation to reach 5 dB at 350 m. With our model of turbulence, a very good agreement between the predictions and the measured values is obtained. A similar result has been previously presented by Daigle[8] who extended the classical coherent acoustic theory by taking into account the amplitude and phase fluctuations. However, in his model the partial coherence between the direct and reflected paths is an adjustable parameter chosen to obtain reasonable agreement with measurements at all frequencies and distances. For low frequencies (below 400 Hz), the fluctuations in phase and amplitude decrease rapidly and atmospheric turbulence is expected to have no significant effects on the sound-pressure level. In Fig. 8 we find that below 400 Hz the numerical

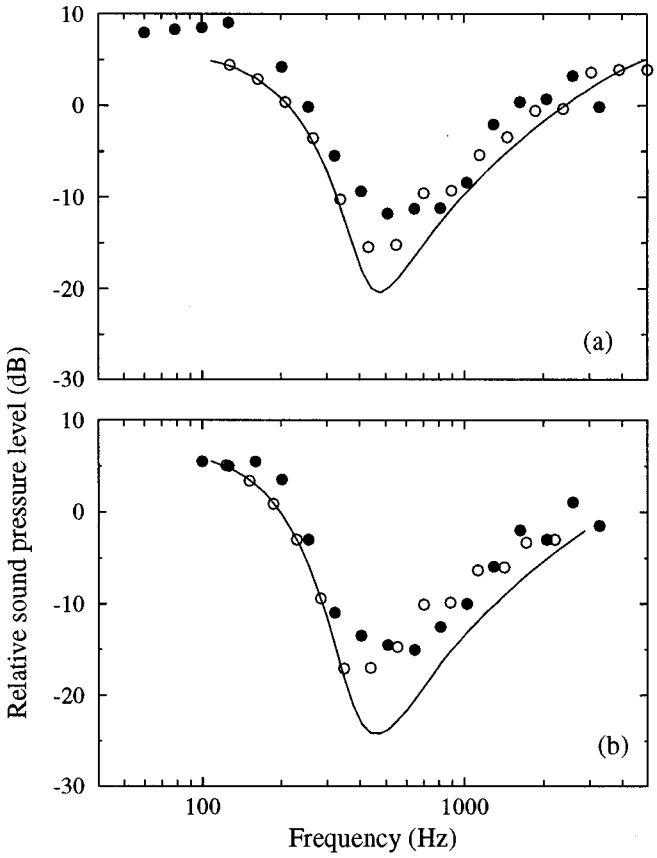

FIG. 8. Relative sound-pressure level spectrum: comparison between Parkin and Scholes's measurements (●), a deterministic calculation (———) and our model (○) [$h_s = 1.8$ m, $h_r = 1.5$ m, (a) $r = 200$ m, (b) $r = 350$ m, $\sigma = 300\,000$ N×m^{-4}×s, $\langle\mu^2\rangle = 2\times10^{-6}$, $L = 1.1$ m].

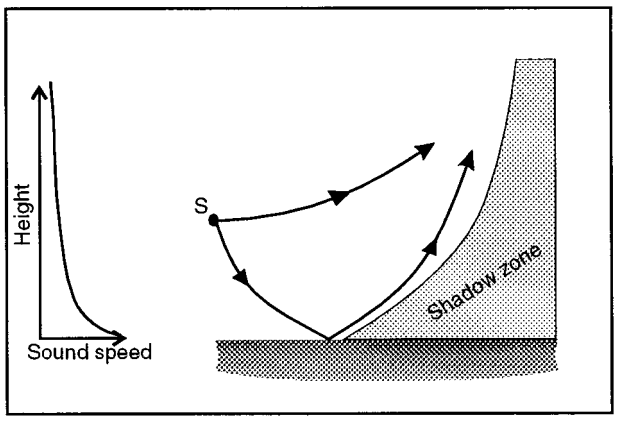

FIG. 9. Sound propagation in a shadow zone.

predictions with turbulence (empty symbols) and without turbulence (solid lines) are identical. We note that these computations underestimate the level in comparison with the outdoor measurements. This difference (<5 dB) between calculated and measured values at low frequencies could be attributed to the local impedance model which fails when the effects of ground waves and surface waves are important. The importance of these waves at low frequencies has been demonstrated by Daigle[8] using the same experimental data.

III. COMPARISONS WITH OUTDOOR MEASUREMENTS IN AN UPWARD REFRACTING ATMOSPHERE

We now consider the propagation of acoustic waves in an upward refracting atmosphere. As illustrated in Fig. 9, an acoustic shadow zone appears in the vicinity of the ground when the sound speed gradient, which depends on the temperature and wind speed profiles, is negative. The ray paths for sound propagating from a source are bent upwards, generating a caustic which delimits the boundary of the shadow zone. For a receiver located in this region there is no direct ray coming from the source, and no direct sound energy can penetrate beyond the edge of the shadow zone. However, in a large number of outdoor experiments, the acoustic levels recorded in the shadow zone are nonnegligible. Sound energy does penetrate this region due to diffraction (at low frequency) and turbulent scattering (at high frequency).[10,19] Here we compare our numerical simulations with the experimental data of Wiener and Keast,[6] which have been already discussed by Piercy *et al.*,[1] Daigle *et al.*,[19] and Gilbert *et al.*[10] In these experiments, the evolution of the relative sound-pressure level with the distance between the source and the receiver is usually described by a step function with three regions associated with different mechanisms of sound wave propagation. The shape of this curve presents a weak dependency with the frequency of the source, but a strong dependency with the degree of upward refraction. First, for short-range propagation, a series of constructive and destructive interferences is noted and there is a spherical spreading of the pressure field. Second, at the edge of the geometric

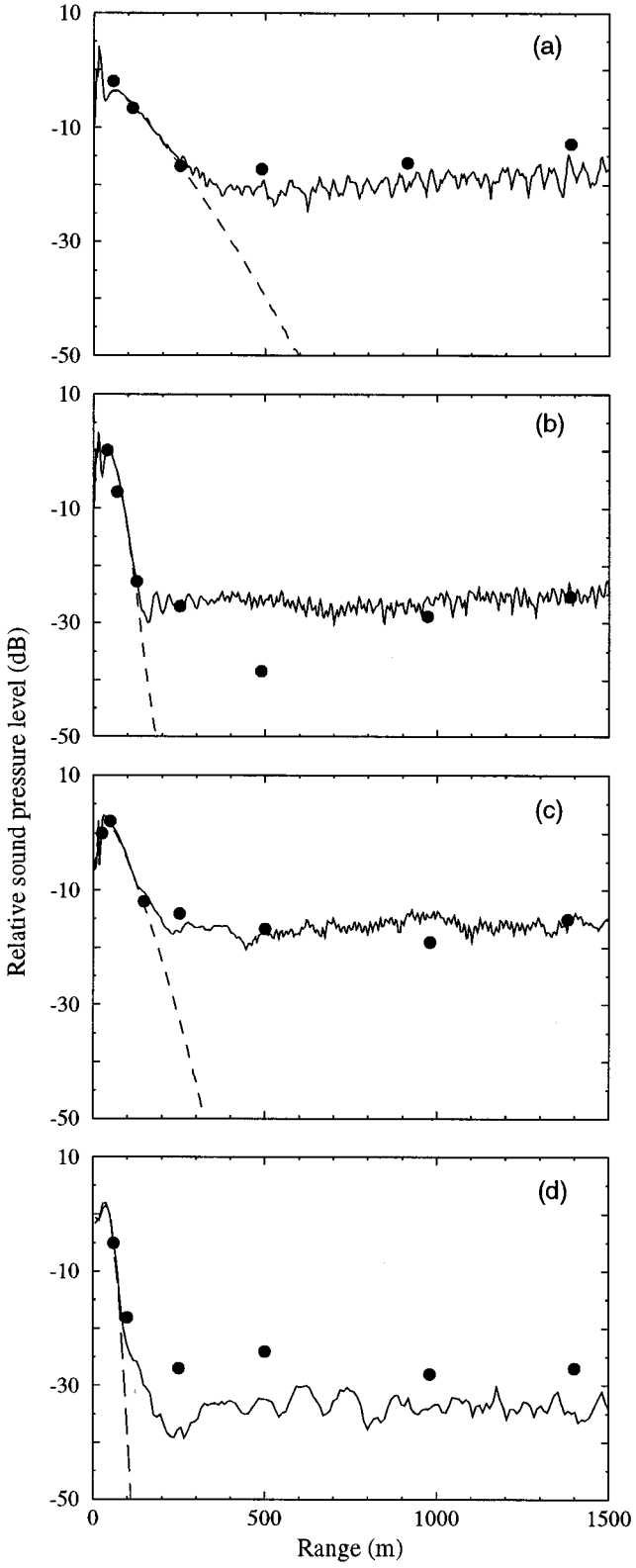

FIG. 10. Relative sound-pressure level: comparisons between Wiener and Keast measurements (●), a deterministic calculation (----) and our model (———) [$h_s=3.7$ m, $h_r=1.5$ m, $\sigma=300\,000$ N×m^{-4}×s, $\langle\mu^2\rangle=2\times10^{-6}$, $L=1.1$ m, $f=424$ Hz (a) weak refractive conditions, (b) strong refractive conditions; $f=848$ Hz (c) weak refractive conditions, (d) strong refractive conditions].

shadow zone, the relative sound pressure decreases abruptly with range until it reaches a uniform level that is the result of atmospheric turbulence. In the third region the relative sound-pressure level follows a plateau at around -20 dB to -30 dB. These typical behaviors are shown in Fig. 10, where we have plotted the experimental data of Wiener and Keast[6] for two frequencies and two profiles of the index of refraction. As noticed by Daigle *et al.*[19] and by Gilbert *et al.*,[10] who give the first quantitative interpretations, the difference between the sound-pressure level in the long-range region and the prediction using a deterministic computation including diffraction effects is a consequence of the scattering of sound by turbulence into the shadow zone.

Wiener and Keast have investigated two situations with upward refraction. The source and the receiver were located, respectively, 3.7 m and 1.5 m over a ground covered with grass (equivalent flow resistivity of 3×10^5 Nm^{-4} s; this value has been used by Gilbert *et al.*[10] in their parabolic equation study of propagation through turbulence). Here we particularly focus on measurements obtained for $\frac{1}{3}$ octave bands centered at frequencies of 424 Hz and 848 Hz. The mean sound speed profiles as well as the turbulence characteristics are those previously used by Gilbert *et al.*:[10]

$$c(z)=\begin{cases} c_0+a\ \ln(z/d), & z\geqslant z_0, \\ c_0+a\ \ln(z_0/d), & z<z_0, \end{cases} \tag{20}$$

where $c_0=340$ m s^{-1}, $z_0=0.01$ m, and $d=6\times10^{-3}$ m. The coefficient a is equal to -0.5 m/s for a weak upward refraction and -2 m/s for a strong upward refraction. For the turbulent parameters, we used the atmospheric parameters given in Gilbert *et al.*,[10] e.g., $\langle\mu^2\rangle=2\times10^{-6}$ and $L=1.1$ m. In Fig. 10 we have plotted the relative sound-pressure level versus the distance of propagation. For each experimental configuration we compare the Wiener and Keast data with the relative sound-pressure level calculated with our parabolic algorithm for a deterministic computation and a turbulent simulation with averaging over 50 realizations.

For short-range propagation there is no noticeable influence of turbulence. The deterministic computation gives the exact values of the outdoor measurements; it confirms the adequate choice of the mean sound speed profiles. When the receiver enters the refractive shadow zone, the effects of the random variations of μ become suddenly important and the deterministic computations largely underestimate the acoustic pressure levels. For long-range propagation the calculations with our turbulence model give a more or less constant value of the relative sound-pressure level, as reported by Gilbert *et al.*[10] for two individual trials. The accuracy of our predictions is generally very good. In particular we find a plateau for the sound pressure in the shadow zone with a correct level except in the case *d* (Fig. 10).

The process of the filling-in of the shadow zone is illustrated in Figs. 11 and 12, where two color maps of the sound-pressure level are shown in the deterministic case, for a particular realization of the turbulent field. For nonturbulent conditions we note, as expected, that the shadow zone is deeper and the transition region sharper at high frequencies [848 Hz; Fig. 12(a)] than at lower frequencies [424 Hz; Fig. 11(a)]. As we can see in Fig. 10, this effect is more pronounced for the case of weak upward refraction than for the case of strong upward refraction. For the turbulent case, the principal mechanism is clearly the scattering of sound from the illuminated region. Especially near the edge of the shadow zone, scattering occurs for preferential directions with respect to the boundary of the shadow zone. The turbulent inhomogeneities with dimensions of size L participate in sound scattering through the angle θ, satisfying the Bragg relation $\theta=2\sin^{-1}(\lambda/2L)$.[7] Consequently, the scattering angle decreases when the frequency of the incident acoustic wave increases. So, for low frequencies, the scattered sound raises the sound level in the shadow zone, including the region near the ground [Fig. 11(b)]. For higher frequencies, when the scattered angle is smaller, we clearly note in Fig. 12(b) the slender aspect of the scattered field, and the sound field near the ground is less influenced by the scattered sound. In this case of a source frequency $f=848$ Hz under strong upward refraction conditions [Fig. 10(d)], our numerical simulation give the global trend of the sound-pressure level in the shadow zone, but the measured levels are underestimated by 5 to 10 dB. Two main factors can explain this discrepancy: (1) the variability of the atmosphere during outdoor sound propagation experiments; (2) the choice of the turbulence model. The numerical simulations are sensitive to the parameters used to describe the mean sound profile (e.g., a, z_0, c_0, d) and the atmospheric turbulence (e.g., $\langle\mu^2\rangle$, L); however, the sound-pressure levels are perfectly predicted for short-range propagation (see Fig. 10), and a variation of 10% of the turbulent variables $\langle\mu^2\rangle$ and L induces no significant modifications (less than 1 dB)[23] so that the variability of the atmosphere is not a relevant explanation. Concerning the model of turbulence, the fluctuations have been considered as scalar and characterized by a single length scale L; it is known that the contributions to the scattering cross section of the temperature and velocity fluctuations are different and depend on the spectral representation of the turbulence.[31] As our simulations seem to indicate that the computed scattering angles are too small, we conjecture that a different spectral representation of the refractive index fluctuations (including a significant ''inertial'' range) would be more appropriate. Preliminary computations have been done to test these ideas,[32,33] and a detailed study of the influence of the model of turbulence will be presented in a forthcoming paper.

In addition to the mean sound-pressure level, it is of interest to study the fluctuations which can be measured around the mean value. In Fig. 13 we have plotted an upper and lower estimation of these variations I_+ and I_- according to the formula

$$I_\pm=10\log[\langle p^2\rangle\pm[\langle(p^2-\langle p^2\rangle)^2\rangle]^{1/2}]. \tag{21}$$

These curves give an idea of the typical mean-square pressure variations we can obtain in the shadow zone, from one realization to another one (up to 10 dB in this case). To complete this analysis, we calculated the normalized mean-square pressure fluctuations $p^2/\langle p^2\rangle$ and the probability distribution of the normalized amplitude fluctuations A/σ_A. When the receiver is located in the line of sight region ($r=10$ m, Fig. 14), the effects of the atmospheric turbulence on sound fluctuations are small. The mean square pressure is

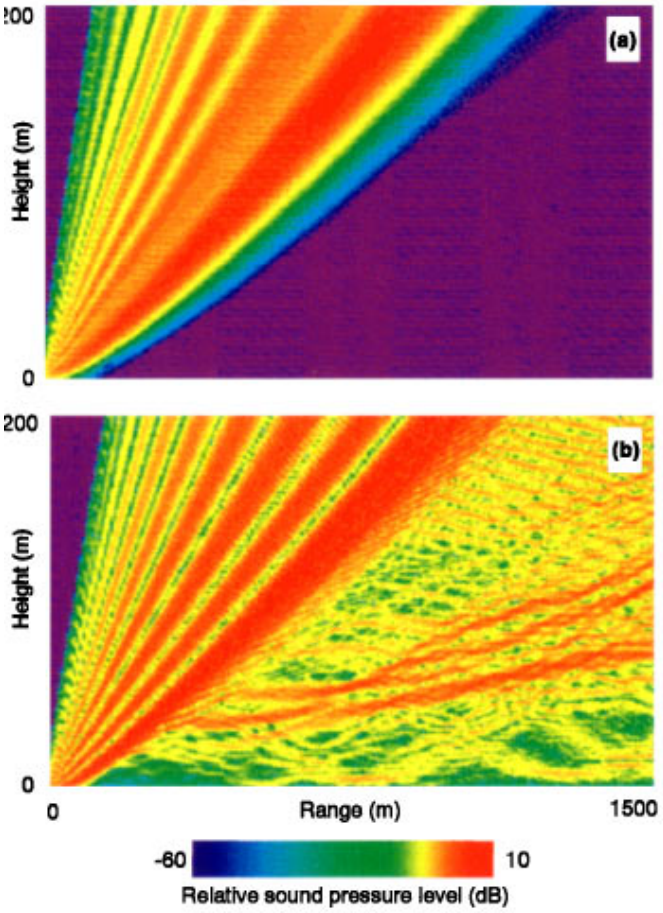

FIG. 11. Relative sound-pressure level in strong refractive conditions for a nonturbulent atmosphere (a) and for one turbulent realization (b) ($f=424$ Hz, $h_s=3.7$ m, $\sigma=300\,000$ N×m^{-4}×s, $\langle\mu^2\rangle=2\times10^{-6}$, $L=1.1$ m).

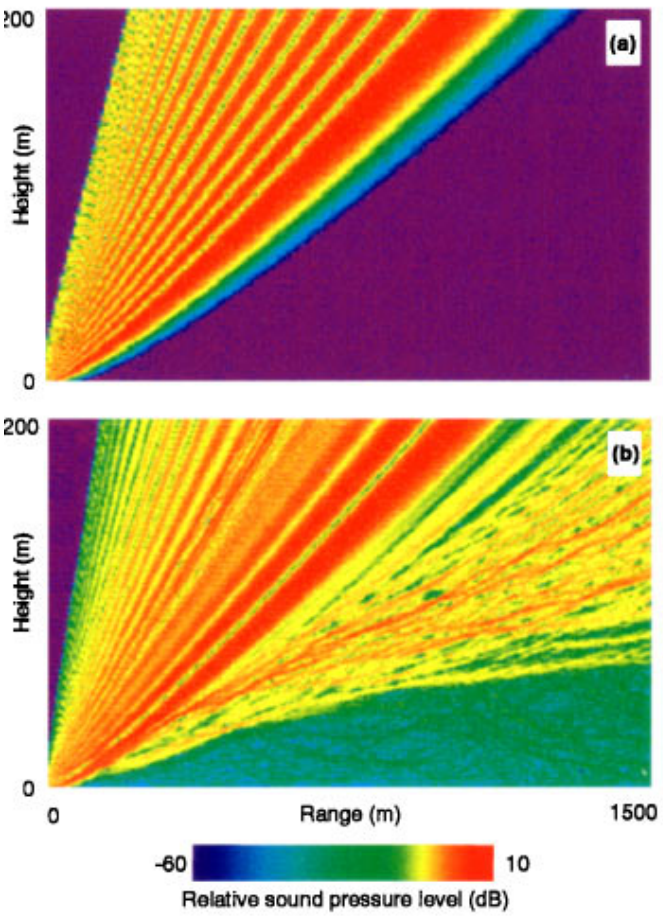

FIG. 12. Relative sound-pressure level in strong refractive conditions for a nonturbulent atmosphere (a) and for one turbulent realization (b) ($f=848$ Hz, $h_s=3.7$ m, $\sigma=300\,000$ N×m^{-4}×s, $\langle\mu^2\rangle=2\times10^{-6}$, $L=1.1$ m).

always of the same order of magnitude as the mean value ($p^2/\langle p^2\rangle=1$), and the amplitude fluctuations are normally distributed according to the expression

$$\mathscr{P}(A)=\frac{1}{\sigma_A\sqrt{2\pi}}\exp\left(-\frac{(A-\langle A\rangle)^2}{2\sigma_A^2}\right). \tag{22}$$

This is in agreement with the previous study of Bass *et al.*[34] When the receiver is located in the shadow zone ($r=300$ m, Fig. 15), the instantaneous evolution of the sound level is totally different. The normalized mean-square pressure $p^2/\langle p^2\rangle$ has an intermittent evolution with a mean level close to zero and sporadic very high peaks (up to 100 times the mean value). The amplitude distribution is no longer a Gaussian distribution; its evolution is very similar to the behavior of the mean square pressure fluctuations measured in free field[35,36] beyond the region of caustics formation. In this case, it has been shown that the Rayleigh–Rice distribution law,[37] valid for a weak turbulence regime, can be extended to a gamma distribution[38] for a strong turbulence regime:

$$\mathscr{P}(A)=\frac{d^p}{\Gamma(p)}\exp(-dA)A^{p-1}, \tag{23}$$

where Γ is the gamma function. The coefficients p and d are obtained from the experimental values of the mean amplitude $\langle A\rangle$ and the variance σ_A^2 by solving the equations

$$\langle A\rangle=p/d, \quad \sigma_A^2=p(p+1)/d^2. \tag{24}$$

In Fig. 15(b) we compare the amplitude distribution obtained from our numerical simulations with the heuristic gamma distribution, and we note a very good agreement.

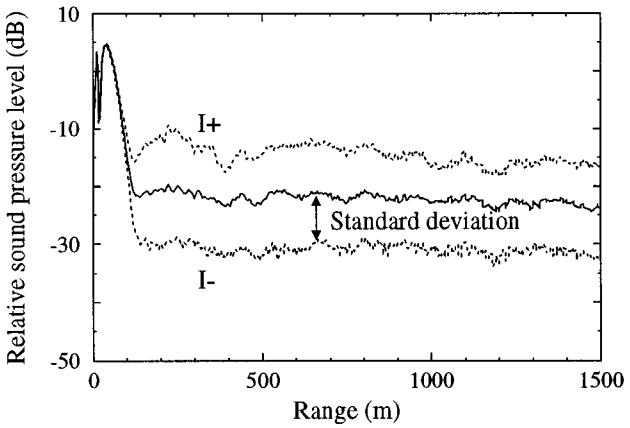

FIG. 13. Relative sound-pressure level and standard deviation for strong refractive conditions (———) $\langle I\rangle$, (----) I_+ and I_- ($f=424$ Hz, $h_s=3.7$ m, $h_r=1.5$ m, $\langle\mu^2\rangle=2\times10^{-6}$, $L=1.1$ m).

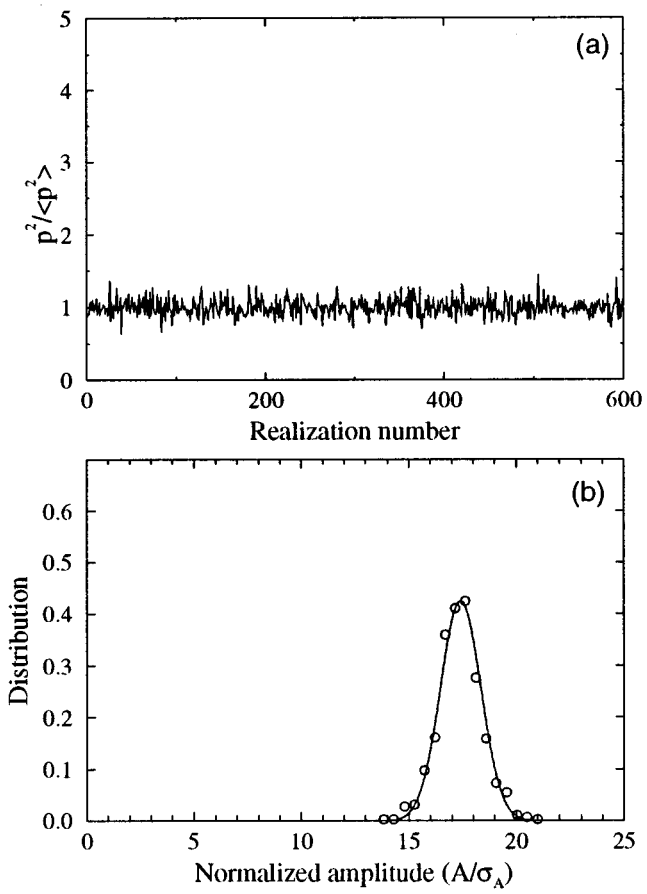

FIG. 14. (a) Normalized mean square pressure and (b) amplitude distribution (———) theoretical law and (○) our computations in the line of sight region ($f=848$ Hz, $h_s=3.7$ m, $h_r=1.5$ m, $r\simeq 10$ m, $\sigma=300\,000$ N×m^{-4}×s, $\langle\mu^2\rangle=2\times10^{-6}$, $L=1.1$ m).

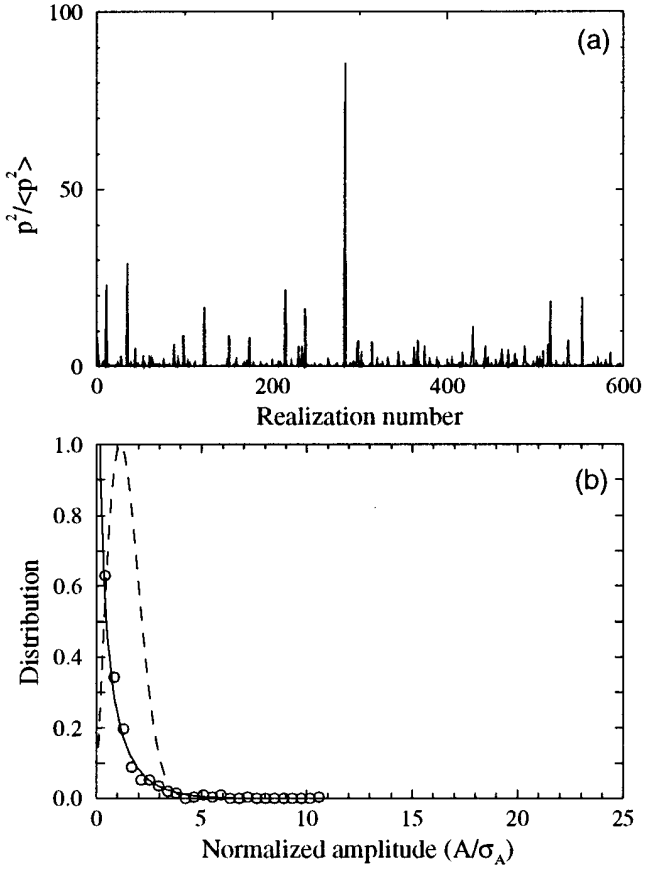

FIG. 15. (a) Normalized mean square pressure and (b) amplitude distribution (———) theoretical gamma law, (----) theoretical Rayleigh–Rice law and (○) our computations in the deep shadow zone ($f=848$ Hz, $h_s=3.7$ m, $h_r=1.5$ m, $r\simeq 300$ m, $\sigma=300\,000$ N×m^{-4}×s, $\langle\mu^2\rangle=2\times10^{-6}$, $L=1.1$ m).

IV. CONCLUSIONS

In this paper we have presented a numerical model to simulate the propagation of acoustic waves in the atmosphere near the ground, with the combined effects of turbulence and mean sound speed gradients. In our technique, the turbulence is represented as a set of realizations of a two-dimensional random field generated by a limited number of Fourier modes. The spectral characteristics of these Fourier modes are chosen according to the statistics of the turbulence. This method requires no *a priori* hypothesis; it only needs measured physical quantities, such as the spatial correlation scales, the variance, and the spectrum of the refractive index fluctuations. For each individual realization, we propagate the acoustic waves using a wide-angle parabolic equation. The ground effects are modeled by a finite complex impedance.

In the first test we considered the case of sound propagation in a nonrefractive atmosphere above ground. For both the rigid and nonrigid ground our numerical simulations are in very good agreement with the experimental data:[3–5] in particular, the mean sound-pressure levels of the minima associated with destructive interferences are well predicted. Scatter plots illustrate different behaviors of the acoustic field when the receiver is located at a point of constructive or destructive interference.

In the second test we studied the propagation of acoustic waves in an upward-refracting atmosphere. Two frequencies were investigated (424 Hz and 848 Hz) as in the experiment reported by Wiener and Keast for weak and strong upward-refracting conditions. In the near field of the source, the turbulence has no significant influence. As soon as the receiver crosses the boundary of the shadow zone, the mean relative sound-pressure level decreases rapidly and reaches a value practically independent of the distance. The existence of this characteristic plateau agrees with the experimental findings; its level is well predicted, except in one case (strong upward conditions with a high-frequency source). One advantage of our numerical approach is that ''instantaneous'' parameters can be obtained, such as amplitude or phase fluctuations. Two attractive results are that the mean square pressure becomes very intermittent in the deep shadow zone, and that the amplitude fluctuations depart strongly from a normal law, and are well represented by a gamma distribution.

The results we have obtained can be considered as very promising; but it must be recognized that the Gaussian model is oversimplified. Improvements can be made along two directions: (1) choosing a better spectral representation of the refractive index fluctuations (von Karman spectrum instead

of a Gaussian derived spectrum), and (2) incorporating the vectorial character of turbulence into our random field generator to take into account that velocity fluctuations as well as temperature fluctuations are present in the atmosphere. Work is currently in progress along these two lines. It is suggested that in future experiments, temperature and velocity spectra have to be measured, as well as their relative contributions to the refractive index fluctuations, so that comparisons with numerical predictions can be made from this view point.

APPENDIX

The sound pressure $p(\mathbf{x})$ at R due to a point source at S placed above a perfectly reflecting boundary (Fig. 4) is the sum of two terms, respectively, associated with the direct and the reflected waves:

$$p(\mathbf{x}) = \frac{A_r}{r_r}\exp(ik_0 r_r + iS_r) + \frac{A_d}{r_d}\exp(ik_0 r_d + iS_d). \quad \text{(A1)}$$

In Eq. (A1), S_d, S_r, and A_d, A_r denote the phase and amplitude of the direct and reflected waves, respectively. When the wave parameter $D = r/(k_0 L^2)$ is much smaller than 1, the mean pressure $\langle p(\mathbf{x})\rangle$ can be evaluated using the geometric approximation method (a detailed analysis can be found in the books of Tatarski[7] and Rytov *et al.*[39]). The ratio between the variance of the amplitude fluctuations and the variance of the phase fluctuations is of the order of D^2. For the conditions of our computations ($D \leqslant 0.2$) this allows us to ignore amplitude as compared to phase fluctuations. Considering that the distances r_r and r_d are of the same order as r, we express the pressure $p(\mathbf{x})$ as

$$p(\mathbf{x}) = \frac{A}{r}\left[\exp(ik_0 r_r + iS_r) + \exp(ik_0 r_d + iS_d)\right]. \quad \text{(A2)}$$

In the geometric approximation, the phase fluctuations of the wave follow a normal law; using the formula $\langle \exp(iS)\rangle = \exp(-\langle S^2\rangle/2)$, we obtain the mean pressure $\langle p(\mathbf{x})\rangle$:

$$\langle p(\mathbf{x})\rangle = \frac{A}{r}\left[\exp(ik_0 r_d)\exp\left(-\frac{\sigma_{S_d}^2}{2}\right) + \exp(ik_0 r_r)\exp\left(-\frac{\sigma_{S_r}^2}{2}\right)\right]. \quad \text{(A3)}$$

$\sigma_{S_d}^2$ and $\sigma_{S_r}^2$ are the phase variance of the direct and reflected waves. From Eqs. (A2) and (A3), the normalized pressure $p/\langle p\rangle$ is expressed as

$$\frac{p}{\langle p\rangle} = \frac{\exp(ik_0 r_r + iS_r) + \exp(ik_0 r_d + iS_d)}{\exp(ik_0 r_d)\exp(-\sigma_{S_d}^2/2) + \exp(ik_0 r_r)\exp(-\sigma_{S_r}^2/2)}. \quad \text{(A4)}$$

From Eq. (A4) it is easy to evaluate the modulus of $p/\langle p\rangle$:

$$\left|\frac{p}{\langle p\rangle}\right| = 2\exp\left(\frac{\sigma_{S_d}^2}{2}\right)\frac{|\cos[(k_0/2)(r_r - r_d) + (S_r - S_d)/2]|}{[1 + \exp(\sigma_{S_d}^2 - \sigma_{S_r}^2) + 2\exp[(\sigma_{S_d}^2 - \sigma_{S_r}^2)/2]\cos\, k_0(r_r - r_d)]^{1/2}}. \quad \text{(A5)}$$

When the receiver is located on a constructive interference, the path difference $r_r - r_d$ is equal to an even multiple of the wavelength. The modulus of $p/\langle p\rangle$ then simplifies to

$$\left|\frac{p}{\langle p\rangle}\right| = 2\exp\left(\frac{\sigma_{S_d}^2}{2}\right)\frac{|\cos[(S_r - S_d)/2]|}{1 + \exp[(\sigma_{S_d}^2 - \sigma_{S_r}^2)/2]}. \quad \text{(A6)}$$

The terms $(S_r - S_d)$ and $\sigma_{S_d}^2 - \sigma_{S_r}^2$ being very small, this last expression reduces to

$$\left|\frac{p}{\langle p\rangle}\right| \simeq \exp\left(\frac{\sigma_{S_d}^2}{2}\right). \quad \text{(A7)}$$

For a medium with single scale inhomogeneities L [Eq. (3)], the phase variances $\sigma_{S_d}^2$ is given in the geometrical approximation by[39]

$$\sigma_{S_d}^2 = \sqrt{\pi}\langle \mu^2\rangle k_0^2 L r, \quad \text{(A8)}$$

so that

$$\left|\frac{p}{\langle p\rangle}\right| \simeq \exp\left(\frac{\sqrt{\pi}}{2}\langle \mu^2\rangle k_0^2 L r\right). \quad \text{(A9)}$$

In the plane $(\mathrm{Re}(p/\langle p\rangle), \mathrm{Im}(p/\langle p\rangle))$ this corresponds to a circle for a fixed position of the receiver.

When the position of the receiver corresponds to a destructive interference, the path difference $(r_r - r_d)$ is equal to an odd multiple of the half-wavelength. Expression (A5) can be then simplified into

$$\left|\frac{p}{\langle p\rangle}\right| = 2\exp\left(\frac{\sigma_{S_d}^2}{2}\right)\frac{|\sin[(S_r - S_d)/2]|}{|1 - \exp[(\sigma_{S_d}^2 - \sigma_{S_r}^2)/2]|}. \quad \text{(A10)}$$

If the differences $(S_r - S_d)$ and $(\sigma_{S_r}^2 - \sigma_{S_d}^2)$ are small, expression (A10) can be approximated by

$$\left|\frac{p}{\langle p\rangle}\right| \simeq 2\exp\left(\frac{\sigma_{S_d}^2}{2}\right)\frac{|S_r - S_d|}{|\sigma_{S_d}^2 - \sigma_{S_r}^2|}. \quad \text{(A11)}$$

Now we are interested in the sign of the real part of $p/\langle p\rangle$. Using the relation $p/\langle p\rangle = (p\langle p\rangle^*)/|\langle p\rangle^2|$, we check the sign of the real part of $p\langle p\rangle^*$. Starting from Eqs. (A2) and (A3), we get

$$\mathrm{Re}\{p\langle p\rangle^*\}=\frac{A^2}{r^2}\{\cos S_r+\cos[S_d+k_0(r_r-r_d)]\}\times\exp\left(-\frac{\sigma_{S_r}^2}{2}\right)+\frac{A^2}{r^2}\{\cos S_d+\cos[S_r+k_0(r_r-r_d)]\}\exp\left(-\frac{\sigma_{S_d}^2}{2}\right). \tag{A12}$$

For a constructive interference we can write

$$\mathrm{Re}\{p\langle p\rangle^*\}=2\frac{A^2}{r^2}\cos\left(\frac{S_r+S_d}{2}\right)\cos\left(\frac{S_r-S_d}{2}\right)\times\left[\exp\left(-\frac{\sigma_{S_r}^2}{2}\right)+\exp\left(-\frac{\sigma_{S_d}^2}{2}\right)\right]. \tag{A13}$$

In this case of a destructive interference the expression (A12) can be simplified as

$$\mathrm{Re}\{p\langle p\rangle^*\}=-2\frac{A^2}{r^2}\sin\left(\frac{S_r+S_d}{2}\right)\sin\left(\frac{S_r-S_d}{2}\right)\times\left[\exp\left(-\frac{\sigma_{S_r}^2}{2}\right)+\exp\left(-\frac{\sigma_{S_d}^2}{2}\right)\right]. \tag{A14}$$

[1] J. E. Piercy, T. F. W. Embleton, and L. C. Sutherland, ''Review of noise propagation in the atmosphere,'' J. Acoust. Soc. Am. **61**, 1403–1418 (1977).

[2] T. F. Embleton and G. A. Daigle, ''Atmospheric propagation,'' in *Aeroacoustics of Flight Vehicles*, edited by H. H. Hubbard (NASA Langley Research Center, Hampton, 1995), Chap. 12.

[3] P. H. Parkin and W. E. Scholes, ''The horizontal propagation of sound from a jet engine close to the ground, at Radlett,'' J. Sound Vib. **1**, 1–13 (1964).

[4] P. H. Parkin and W. E. Scholes, ''The horizontal propagation of sound from a jet engine close to the ground, at Hatfield,'' J. Sound Vib. **2**, 353–374 (1965).

[5] G. A. Daigle, J. E. Piercy, and T. F. W. Embleton, ''Effects of atmospheric turbulence on the interference of sound waves near a hard boundary,'' J. Acoust. Soc. Am. **64**, 622–630 (1978).

[6] F. M. Wiener and D. N. Keast, ''Experimental study of the propagation of sound over ground,'' J. Acoust. Soc. Am. **31**, 724–733 (1959).

[7] V. I. Tatarskii, *The Effect of a Turbulent Atmosphere on Wave Propagation* (I.P.S.T Keter, Jerusalem, 1971).

[8] G. A. Daigle, ''Effects of atmospheric turbulence on the interference of sound waves above a finite impedance boundary,'' J. Acoust. Soc. Am. **65**, 45–49 (1979).

[9] L. A. Chernov, *Wave Propagation in a Random Medium* (McGraw-Hill, New York, 1960).

[10] K. E. Gilbert, R. Raspet, and X. Di, ''Calculation of turbulence effects in an upward-refracting atmosphere,'' J. Acoust. Soc. Am. **87**, 2428–2437 (1990).

[11] D. Juvé, Ph. Blanc-Benon, and G. Comte-Bellot, ''Transmission of acoustic waves through mixing layers and 2D isotropic turbulence,'' in *Turbulence and Coherent Structures*, edited by O. Métais and M. Lesieur (Kluwer, Boston, 1990), pp. 367–384.

[12] W. E. McBride, H. E. Bass, R. Raspet, and K. E. Gilbert, ''Scattering of sound by atmospheric turbulence: A numerical simulation above a complex impedance boundary,'' J. Acoust. Soc. Am. **90**, 3314–3325 (1991).

[13] Ph. Blanc-Benon, D. Juvé, M. Karweit, and G. Comte-Bellot, ''Simulation numérique de la propagation des ondes acoustiques à travers une turbulence cinématique,'' J. d'Acoust. **3**, 1–8 (1990).

[14] Ph. Blanc-Benon, D. Juvé, and G. Comte-Bellot, ''Occurrence of caustics for high-frequency acoustic waves propagating through turbulent fields,'' Theor. Comput. Fluid Dynam. **2**, 271–278 (1991).

[15] Y. Hugon-Jeannin, ''Simulation numérique de la propagation d'ondes acoustiques en milieu turbulent,'' Ph.D. thesis, Ecole Centrale de Lyon, 1992, No. 92-37.

[16] D. Juvé, Ph. Blanc-Benon, and P. Chevret, ''Numerical simulation of sound propagation through a turbulent atmosphere,'' in *Proceedings of the Fifth International Symposium on Long Range Sound Propagation*, Milton Keynes, UK, 24–26 May 1992, pp. 282–296.

[17] M. Karweit, Ph. Blanc-Benon, D. Juvé, and G. Comte-Bellot, ''Simulation of the propagation of an acoustic wave through a turbulent velocity field: A study of phase variance,'' J. Acoust. Soc. Am. **89**, 52–62 (1991).

[18] G. A. Daigle, J. E. Piercy, and T. F. W. Embleton, ''Line-of-sight propagation through atmospheric turbulence near the ground,'' J. Acoust. Soc. Am. **74**, 1505–1513 (1983).

[19] G. A. Daigle, T. F. Embleton, and J. E. Piercy, ''Propagation of sound in the presence of gradients and turbulence near the ground,'' J. Acoust. Soc. Am. **79**, 613–627 (1986).

[20] D. I. Havelock, X. Di, G. A. Daigle, and M. R. Stinson, ''Spatial coherence of a sound field in a refractive shadow: Comparison of simulation and experiment,'' J. Acoust. Soc. Am. **98**, 2289–2302 (1995).

[21] D. J. Thomson and N. R. Chapman, ''A wide-angle split-step algorithm for the parabolic equation,'' J. Acoust. Soc. Am. **74**, 1848–1854 (1983).

[22] M. D. Collins, ''A split-step Padé solution for the parabolic equation,'' J. Acoust. Soc. Am. **93**, 1736–1742 (1993).

[23] P. Chevret, ''Simulation numérique des effets de la turbulence sur la propagation du son dans l'atmosphère,'' Ph.D. thesis, Ecole Centrale de Lyon, 1994, No. 94-18.

[24] K. E. Gilbert and M. J. White, ''Application of the parabolic equation to sound propagation in a refracting atmosphere,'' J. Acoust. Soc. Am. **85**, 630–637 (1989).

[25] K. E. Gilbert and X. Di, ''A fast Green's function method for one-way sound propagation in the atmosphere,'' J. Acoust. Soc. Am. **94**, 2343–2352 (1993).

[26] X. Di and K. E. Gilbert, ''The effect of turbulence and irregular terrain on outdoor sound propagation,'' in *Proceedings of the Sixth International Symposium on Long Range Sound Propagation*, Ottawa, Canada, 12–14 June 1994, pp. 315–328.

[27] Y. Saad and D. Lee, ''A new algorithm for solving the wide angle wave equation,'' in *Computational Acoustics*, edited by D. Lee, R. L. Sternberg, and M. H. Schultz (Elsevier Science, Amsterdam, 1988), pp. 119–132.

[28] W. H. Press, B. P. Flannery, S. K. Teutolski, and W. J. Vetterling, *Numerical Recipes. The Art of Scientific Computing* (Cambridge U.P., Cambridge, MA, 1986).

[29] K. Attenborough, S. I. Hayek, and J. M. Lawther, ''Propagation of sound above a porous half-space,'' J. Acoust. Soc. Am. **68**, 1493–1501 (1980).

[30] M. E. Delany and E. N. Bazley, ''Acoustical properties of fibrous absorbent materials,'' Appl. Acoust. **3**, 105–116 (1970).

[31] V. E. Ostashev, ''Sound propagation and scattering in a media with random inhomogeneities of sound speed, density, and medium velocity,'' Waves Random Media **4**, 403–428 (1994).

[32] D. Juvé, Ph. Blanc-Benon, and P. Chevret, ''Sound propagation through a turbulent atmosphere: influence of the turbulence model,'' in *Proceedings of the Sixth International Symposium on Long Range Sound Propagation*, Ottawa, Canada, 12–14 June 1994, pp. 270–282.

[33] Ph. Blanc-Benon, D. Juvé, and P. Chevret, ''On the influence of the turbulence modeling for atmospheric sound propagation,'' J. Acoust. Soc. Am. **98**, 2924 (1995).

[34] H. E. Bass, L. N. Bolen, R. Raspet, W. McBride, and J. Noble, ''Acoustic propagation through a turbulent atmosphere: Experimental characterization,'' J. Acoust. Soc. Am. **90**, 3307–3313 (1991).

[35] Ph. Blanc-Benon and D. Juvé, ''Intensity fluctuations of spherical acoustic waves propagating through thermal turbulence,'' Waves Random Media **3**, 71–83 (1993).

[36] T. E. Ewart and D. B. Percival, ''Forward scattered waves in random media: The probability distribution of intensity,'' J. Acoust. Soc. Am. **80**, 1745–1753 (1986).

[37] J. W. Strohbehn, T. Wang, and J. P. Speck, ''On the probability distribution of line-of-sight fluctuations of optical signals,'' Radio Sci. **10**(1), 59–70 (1975).

[38] E. W. Stacy, ''A generalization of the gamma distribution,'' Ann. Math. Stat. **33**, 1187–1192 (1962).

[39] S. M. Rytov, Yu. A. Kravtsov, and V. I. Tatarskii, *Elements of Random Process Theory: Principles of Statistical Radiophysics* (Springer-Verlag, Berlin, 1987), Vol. 4.